6th European Conference on Computational Mechanics (ECCM 6)
7th European Conference on Computational Fluid Dynamics (ECFD 7)
11-15 June 2018, Glasgow, UK

OPTIMIZATION UNDER UNCERTAINTIES USING THE CONTINUOUS ADJOINT METHOD AND POLYNOMIAL CHAOS EXPANSION

Athanasios G. Liatsikouras[1,2], Varvara G. Asouti[2] and Kyriakos C. Giannakoglou[2]

[1] ESI Software Germany GmbH, Essen, Germany
thanasis.liatsi@gmail.com

[2] National Technical University of Athens (NTUA)
School of Mechanical Engineering, Parallel CFD & Optimization Unit, Greece
vasouti@mail.ntua.gr, kgianna@central.ntua.gr

Key words: Robust Design, Polynomial Chaos Expansion, Uncertainty Quantification, Continuous Adjoint

Abstract. Uncertainties associated with either the operating conditions and/or manufacturing imperfections frequently affect the results of design/optimization methods in various engineering fields. This paper deals with optimization under uncertainties related to the flow conditions and is based on the non-intrusive Polynomial Chaos Expansion (PCE). In previous work by the same group of authors, the non–intrusive PCE was combined with evolutionary algorithms [1, 2]; in contrast, in this work, the optimization is performed by a gradient–based algorithm. The role of PCE is to compute the first and second statistical moments of the quantity of interest. Working, though, with a gradient–based method, the gradient of these statistical moments with respect to the design variables must be computed too and this is made possibly by implementing the continuous adjoint technique. This paper presents optimizations under uncertainties of a) a heat transfer system, namely a lid–driven cavity with one blowing and one suction jet for the maximization of the heat extracted through the upper moving wall by computing the optimal locations of the jets, with uncertainties related to their operating conditions and b) a car model aiming at minimum drag, in which the design variables are the control points of a volumetric B–Splines lattice and the uncertain variable is the freestream velocity.

1 INTRODUCTION

During the last years, research is focused on the development of tools for the analysis and design–optimization in various engineering fields. Most of these tools solve problems with fixed operating conditions. However, this is not the case in real–world applications where the flow conditions may vary and/or the manufactured shape may deviate from the CAD model. For instance, the drag force of a car is affected by the unforeseen presence of side–wind. To take this into consideration, the development of algorithms for analysis under uncertainties related to flow conditions and/or manufacturing imperfections are necessary.

The term Uncertainty Quantification (UQ) refers to mathematical ways of quantifying the effect of the uncertainty on the quantity of interest (QoI, denoted by F). In the literature, there are several methods for computing/approximating the mean value and the standard deviation of a function. Each of them has its pros and cons. A well–known stochastic technique is the Monte–Carlo (MC) one [3] but, for large–scale problems, this is prohibitively expensive in terms of CPU. To reduce its cost, the Quasi–MC [4] and Latin–Hypercube Sampling techniques [5] have alternatively been proposed.

Compared to all MC variants, a much more efficient method to deal with the same problem is the method of statistical moments [6]. In the latter, the second derivatives of F w.r.t. the uncertain variables are required in order to compute the first two statistical moments of F with second order–accuracy, [6, 7].

Another way to model uncertainties in engineering applications is the polynomial chaos expansion (PCE) [8]. This is based on the use of orthogonal polynomials and can be either intrusive or non–intrusive, depending on whether the governing equations are altered or not. The intrusive PCE introduces the uncertainty in the mathematical model, leading to a new system of PDEs that must be solved numerically. On the other hand, in non–intrusive PCE, the standard evaluation software, without any intervention, is used to perform the analysis and compute F at some pre–defined data sets. The latter are the so–called Gaussian nodes, determined by the Gauss Quadrature (GQ) integration rules.

This paper is dealing with the optimization under flow uncertainties by making use of the non–intrusive PCE method assisted by the continuous adjoint technique [9, 10]. The latter computes the gradient of the QoI w.r.t. the design variables at the Gaussian nodes and the non–intrusive PCE method is used to compute the objective function and its gradient for the robust design problem. The first case studied in this paper is a heat transfer problem representative of configurations used in cooling machine components. The target is to find the optimal positions of jets so as to increase the heat transfer in the presence of uncertainties related to their operating conditions. The second case, this paper is dealing with, is the shape optimization under uncertainties of a car model aiming at minimum drag.

2 GRADIENT–BASED OPTIMIZATION UNDER UNCERTAINTIES

2.1 UQ using Non–Intrusive PCE and Gradient Computation

Let $F(\vec{\xi},\vec{b})$ be the QoI affected by the stochastic variable vector $\vec{\xi}$ for which $w(\vec{\xi})$ is the probability density function (a normal distribution is, herein, assumed) and the design variable vector $\vec{b}$. According to the PCE [11], F can be approximated by a linear combination of $C{=}(M+q)!/(M!q!)$ orthogonal normalized Hermite polynomials $H_i(\vec{\xi})$ of degree i as

$$F(\vec{\xi},\vec{b}) \approx \sum_{i=0}^{C} \alpha_i(\vec{b}) H_i(\vec{\xi}) \tag{1}$$

where $\alpha_i, i \in [0,C]$ are the unknown PCE coefficients, M stands for the number of stochastic variables and q for the chaos order. The first two statistical moments of F, i.e. its mean value and variance, can be written as

$$\mu_F(\vec{b}) = \int_{-\infty}^{+\infty} F(\vec{\xi},\vec{b}) w(\vec{\xi}) d\vec{\xi} = \alpha_0(\vec{b}), \quad \sigma_F^2(\vec{b}) = \int_{-\infty}^{+\infty} \Big(F(\vec{\xi},\vec{b}) - \mu_F(\vec{b})\Big)^2 w(\vec{\xi}) d\vec{\xi} = \sum_{i=1}^{C} \alpha_i^2(\vec{b}) \tag{2}$$

where

$$\alpha_i(\vec{b}) = \int_{-\infty}^{+\infty} F(\vec{\xi},\vec{b}) H_i(\vec{\xi}) w(\vec{\xi}) d\vec{\xi} = \sum_{j=1}^{P} t_j H_i(z_j) F(z_j,\vec{b}) \tag{3}$$

The integrations required by eq. (3) can be performed by the GQ formula [12], after computing F at $P{=}(q+1)^M$ Gaussian nodes z_j, where t_j for the weights indicated by the Gauss integration rules.

Having computed the statistical moments of $F(\vec{\xi})$, the objective function ($\hat{F}$) to be maximized/minimized for the problem under uncertainties is defined as

$$\hat{F} = \mu_F + \kappa \sigma_F^2 \tag{4}$$

where κ is a user–defined weight.

To perform the optimization with a gradient–based method, the derivatives of the statistical moments of $\hat{F}$ w.r.t. the design variables $\vec{b}$

$$\frac{\delta \hat{F}}{\delta \vec{b}} = \frac{\delta \mu_F}{\delta \vec{b}} + \kappa \frac{\delta \sigma_F^2}{\delta \vec{b}} \tag{5}$$

should be computed. From eq. (1),

$$\frac{\delta F(\vec{\xi},\vec{b})}{\delta \vec{b}} \approx \sum_{i=0}^{C} \frac{\delta \alpha_i(\vec{b})}{\delta \vec{b}} H_i(\vec{\xi}) \tag{6}$$

and, by differentiating eq. (2),

$$\frac{\delta \mu_F(\vec{b})}{\delta \vec{b}} = \frac{\delta \alpha_0(\vec{b})}{\delta \vec{b}}, \quad \frac{\delta \sigma_F^2(\vec{b})}{\delta \vec{b}} = 2 \sum_{i=1}^{C} \alpha_i(\vec{b}) \frac{\delta \alpha_i(\vec{b})}{\delta \vec{b}} \tag{7}$$

where, from eq. (3),

$$\frac{\delta\alpha_i(\vec{b})}{\delta\vec{b}} = \int_{-\infty}^{+\infty} \frac{\delta F(\vec{\xi},\vec{b})}{\delta\vec{b}} H_i(\vec{\xi}) w(\vec{\xi}) d\vec{\xi} = \sum_{j=1}^{P} t_j H_i(z_j) \frac{\delta F(z_j,\vec{b})}{\delta\vec{b}} \tag{8}$$

According to eq. (8), the required derivatives $\delta\alpha_i(\vec{b})/\delta\vec{b}$ result as the weighted sum of the derivatives of F, computed by the adjoint method, at the P points z_j within the domain of integration. Thus, the adjoint method should merely provide $\delta F(\vec{b})/\delta\vec{b}$ at the Gaussian nodes.

2.2 Gradient–based Optimization Under Uncertainties

Starting from an initial value–set $\vec{b}$, the basic steps of the optimization under uncertainties are described below:

1. Solve the flow and adjoint equations to compute F and its gradient at the Gaussian nodes z_j, at the cost of P flow and P adjoint solutions, or approximately $2P$ equivalent flow solutions (EFS), in total.
2. Compute the statistical moments of F from eq. (2) and their gradients from eq. (7).
3. Compute $\hat{F}$ and its gradient w.r.t. $\vec{b}$ using eqs. (4) and (5), respectively.
4. Update $\vec{b}$ by performing a descent step.
5. Unless the stopping criterion is met, go to step 1.

3 HEAT TRANSFER MAXIMIZATION IN A LID–DRIVEN CAVITY FLOW

3.1 Case Description

The first application of this paper is the design under uncertainties of the jet system of a square cavity, for maximum heat transfer through the lid (moving upper wall), fig. 1. The length of each side is L. In the cavity, fluid of specific properties is enclosed. The bottom wall is at constant normalized temperature T_{th}/T_c=1. The moving upper wall (mw) has a constant temperature $T_{mw} = 0.4285T_c$ and it is sliding to the right with a constant normalized velocity v_{mw}=1, making the fluid recirculate inside the cavity. Two steady jets are placed at two locations along both vertical adiabatic walls for controlling the heat transfer. The jet on the left wall (Jet 1) provides fluid with a constant velocity equal to $v_{jet} = 0.6v_{mw}$, zero angle and temperature $T_{jet} = 0.5714T_c$. The same amount of mass flux entering the cavity is extracted through the jet on the right side (Jet 2). The aim of this design problem is to find the optimal position of each jet for the aforementioned objective. The latter is the QoI in this problem, computed along the moving wall as

$$F = \int_{S_{mw}} \frac{\partial T}{\partial x_i} n_i dS \tag{9}$$

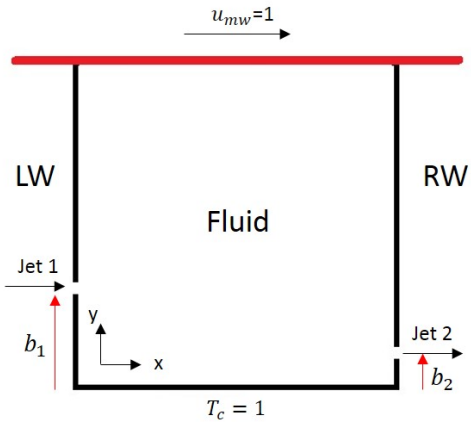

Figure 1: Geometry of the cavity. Fluid is blowing from orifice labelled 'Jet 1' normal to the left wall. The same amount of fluid is extracted from the orifice 'Jet 2' on the right wall.

where n_i is the i–th component of the outward unit normal vector at the boundary.

Two design variables $\vec{b} = (b_1, b_2) \in \mathbb{R}^N = \mathbb{R}^2$, standing for the positions of the jets on the left and right walls, are considered. The width of each jet is $d = 0.05L$. The initial normalized jet positions are $(b_1/L, b_2/L) = (0.3, 0.1)$, measured from the bottom wall. The heat transfer inside the cavity is determined from the temperature difference between the upper and bottom wall. The flow inside the cavity is laminar with Reynolds number equal to Re=661.8, based on L and v_{mw}.

3.2 Flow Equations

The governing PDEs, including the energy equation for the laminar flow of an incompressible fluid, are

$$\begin{aligned} R^p &= -\frac{\partial v_j}{\partial x_j} = 0 \\ R_i^v &= v_j \frac{\partial v_i}{\partial x_j} - \frac{\partial}{\partial x_j}\left[\nu\left(\frac{\partial v_i}{\partial x_j} + \frac{\partial v_j}{\partial x_i}\right)\right] + \frac{\partial p}{\partial x_i} = 0 \\ R^T &= c_p v_j \frac{\partial T}{\partial x_j} - c_p \frac{\partial}{\partial x_j}\left(\frac{\nu}{Pr}\frac{\partial T}{\partial x_j}\right) = 0 \end{aligned} \tag{10}$$

where v_i are the components of the velocity vector, p is the static pressure, c_p the heat capacity and Pr the Prandtl number.

The existence of jets asks for special boundary conditions for the velocity field on both sides of the cavity. A combination of two differentiable, logistic functions is utilized to model the velocity profile of each jet, centered at b_n, as follows

$$\phi(y, b_n) = \frac{1}{1 + e^{-k[y-(b_n - d/2)]}}\left(1 - \frac{1}{1 + e^{-k[y-(b_n + d/2)]}}\right) \tag{11}$$

where k is a coefficient controlling the shape of the logistic functions. Table 1 summarizes the boundary conditions for the left (LW) and right (RW) wall (jet and impermeable wall).

Wall	v_i	p	T
LW	$v_1 n_1(1-\phi) + (v_1 n_1 - v_{jet})\phi = 0$	$\frac{\partial p}{\partial n}(1-\phi) + p\phi = 0$	$\frac{\partial T}{\partial n}(1-\phi) + (T - T_{jet})\phi = 0$
RW	$v_1 n_1(1-\phi) + (v_1 n_1 - v_{jet})\phi = 0$	$\frac{\partial p}{\partial n} = 0$	$\frac{\partial T}{\partial n} = 0$

Table 1: Boundary conditions along the walls and their jets for the primal problem (v_2=0 at both walls).

3.3 Development of the Continuous Adjoint Method

To compute the gradient of the QoI F, the development of the adjoint method starts from

$$F_{aug} = F + \int_\Omega u_i R_i^v d\Omega + \int_\Omega q R^p d\Omega + \int_\Omega T^a R^T d\Omega \tag{12}$$

where u_i are the components of the adjoint velocity, q the adjoint pressure and T^a the adjoint temperature. Differentiating eq. (12) w.r.t. the design variables, yields

$$\frac{\delta F_{aug}}{\delta b_n} = \frac{\delta F}{\delta b_n} + \int_\Omega q \frac{\partial R^p}{\partial b_n} d\Omega + \int_\Omega u_i \frac{\partial R_i^v}{\partial b_n} d\Omega + \int_\Omega T_a \frac{\partial R^T}{\partial b_n} d\Omega \tag{13}$$

After differentiating eqs. (10), expanding and rearranging terms in eq. (13), the computation of the gradient becomes independent of variations in (v, p, T) by setting their multipliers to zero. This gives rise to the field adjoint equations

$$\begin{aligned}
R^q &= -\frac{\partial u_j}{\partial x_j} = 0 \\
R_i^u &= u_j \frac{\partial v_j}{\partial x_i} - v_j \frac{\partial u_i}{\partial x_j} - \frac{\partial}{\partial x_j}\left[\nu\left(\frac{\partial u_i}{\partial x_j} + \frac{\partial u_j}{\partial x_i}\right)\right] + \frac{\partial q}{\partial x_i} + c_p T^a \frac{\partial T}{\partial x_i} = 0 \\
R^{T^a} &= -c_p v_j \frac{\partial T^a}{\partial x_j} - c_p \frac{\partial}{\partial x_j}\left(\frac{\nu}{Pr}\frac{\partial T^a}{\partial x_j}\right) = 0
\end{aligned} \tag{14}$$

After satisfying these equations and their boundary conditions (derived in a similar way though omitted in the interest of space), the remaining terms in eq. (13) form the gradient of F which takes the form

$$\frac{\delta F}{\delta b_1} = \begin{cases} \int_{S_{LW}} \Big[-q n_1 v_{jet} + \nu\big(\frac{\partial u_1}{\partial x_j} + \frac{\partial u_j}{\partial x_1}\big) n_j v_{jet} + \\ \big(c_p T^a v_j n_j + \frac{c_p}{Pr}\nu\frac{\partial T^a}{\partial x_j} n_j\big)\frac{1}{\phi}\big(\frac{\partial T}{\partial x_j} n_j - T + T_{jet}\big)\Big]\frac{\partial \phi}{\partial b_1} dS & \text{, if } \phi \neq 0 \\ \\ \int_{S_{LW}} \Big[-q n_1 v_{jet} + \nu\big(\frac{\partial u_1}{\partial x_j} + \frac{\partial u_j}{\partial x_1}\big) n_j v_{jet} - \\ \frac{c_p}{Pr}\nu T^a \frac{1}{1-\phi}\big(\frac{\partial T}{\partial x_j} n_j - T + T_{jet}\big)\Big]\frac{\partial \phi}{\partial b_1} dS & \text{, if } \phi = 0 \end{cases}$$

$$\frac{\delta F}{\delta b_2} = \int_{S_{RW}} \Big[-q n_1 v_{jet} + \nu\big(\frac{\partial u_1}{\partial x_j} + \frac{\partial u_j}{\partial x_1}\big) n_j v_{jet}\Big]\frac{\partial \phi}{\partial b_2} dS \tag{15}$$

In eq. (15), $\phi = 1$ corresponds to the center of the jet whereas $\phi = 0$ is over the impermeable wall. Recall that, eq. (15) gives the gradient of the QoI w.r.t. b_n; in an optimization problem without uncertainties, this becomes the gradient of the objective function itself.

3.4 Optimization Under Uncertainties

In this section, the optimization with and without uncertainties in the aforementioned lid–driven cavity case is performed. The goal of the optimization under uncertainties is to maximize $\hat{F}$ (given by eq. (4), with $\kappa=-6$), where the QoI is given by eq. (9), by finding the optimal positions of the jets. The velocity magnitude and temperature of Jet 1 and the temperature of the bottom wall are considered as uncertain variables. It is assumed that all uncertain variables follow normal distributions with known mean values and standard deviations as in Table 2. Initially, before proceeding with the optimization, a UQ study is performed for different chaos orders. Results are summarized in Table 3, showing that q=2 is a good compromise in terms of computational cost and accuracy. With q=2, for each optimization cycle 27 flow and 27 adjoint runs are required.

Uncertain Variable	mean value	standard deviation
v_{jet}/v_{mw}	0.6	0.07
T_{jet}/T_c	0.5714	0.003
T_{th}/T_c	1	0.002

Table 2: The heat transfer cavity problem: Mean values and standard deviations of the three uncertain variables. All of them follow normal distributions.

Chaos Order	μ_F/F_{ref}	σ_F/F_{ref}	#Flow Runs
2	1	0.01656	27
3	1	0.01660	64
4	1	0.01663	125

Table 3: The heat transfer cavity problem: Mean value and standard deviation of the heat flux for the initial position of the jets. Computations performed using the non–intrusive PCE method. Tabulated values are normalized using the reference value of F_{ref}=2.6622. The last column stands for the computational cost per UQ.

Once the UQ studies have been completed, the next step is to proceed to the adjoint–based optimization with and without uncertainties. The optimization under uncertainties is carried out for chaos orders q=2 and q=3. The convergence histories of these runs are shown in fig. 2. The increase in the QoI, in the design without uncertainties is about 54.5% and is achieved in less than 10 cycles. An increase in $\hat{F}$ of approximately 51%, in 6 optimization cycles, is achieved in the presence of uncertainties. In Table 4, the initial and the optimal sets of design variables (positions of jets) for each optimization run (with and without uncertainties) are tabulated. Finally, the temperature distribution of the optimal set of design variables, generated from the optimization with and without uncertainties, is presented in fig. 3. The fluid blowing from the Jet 1, if located at the computed optimal position, increases the mean temperature inside the cavity from 438K to 482K. This explains the increase in $\hat{F}$, since the temperature difference between the fluid and the moving lid is higher, increasing thus the heat transfer.

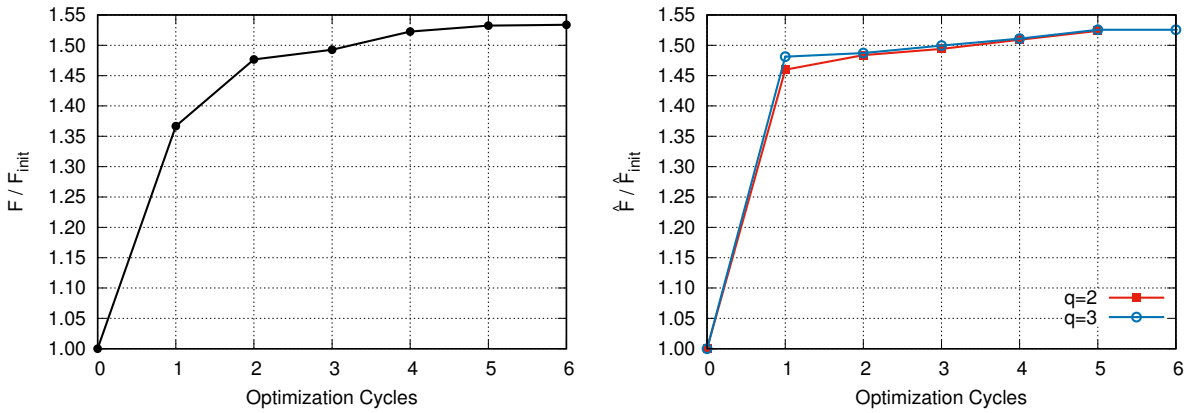

Figure 2: The heat transfer cavity problem: Convergence history of the optimization without uncertainties (left) and with uncertainties for chaos order q=2 and q=3 (right).

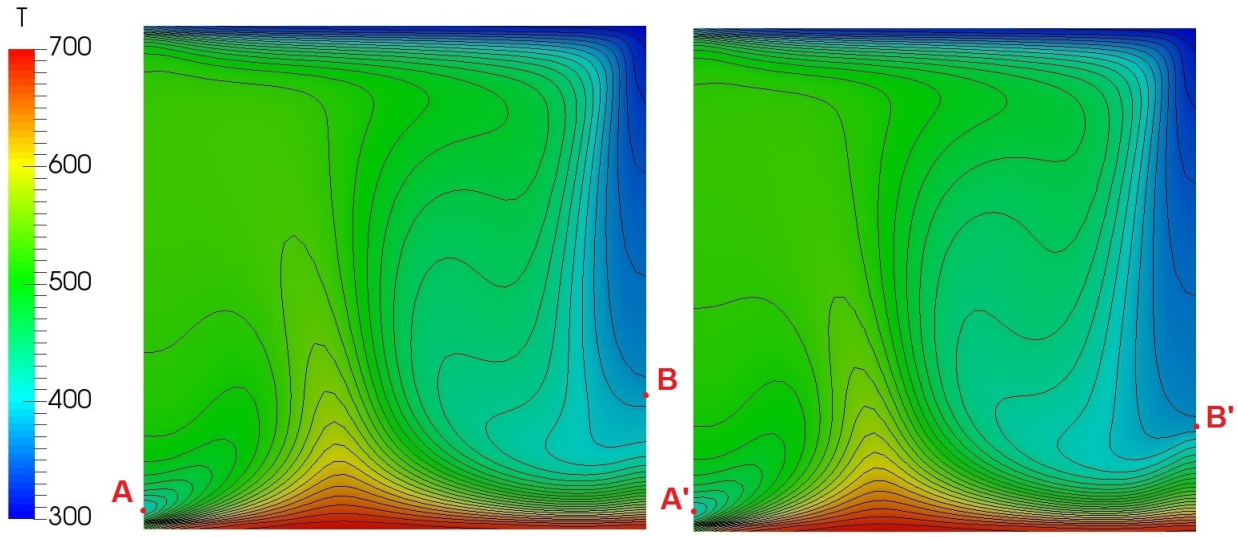

Figure 3: The heat transfer cavity problem: Temperature distribution for the optimal set of design variables resulting from the optimization without (left) and with (right) uncertainties. The optimal positions of the jets are marked with capital letters. The simulation is performed for the mean value of the uncertain variables just for the purpose of comparison.

Case	b_1/L	b_2/L	μ_F/F_{ref}	σ_F/F_{ref}
Baseline	0.300	0.100	1.	0.01656
Optimized (without uncertainty)	0.025	0.267	1.5451	0.01713
Optimized (q=2)	0.025	0.201	1.4465	0.01521
Optimized (q=3)	0.025	0.204	1.4465	0.01514

Table 4: The heat transfer cavity problem: Normalized set of design variables, mean value and standard deviation for the initial and the optimal positions of the jets for each optimization run. Tabulated values are normalized using F_{ref}.

4 OPTIMIZATION UNDER UNCERTAINTIES OF THE DRIVAER CAR

The second case is dealing with the UQ and the shape optimization under uncertainties of the DrivAer car [13] model (fig. 4). The half car of the fast–back configuration with a smooth underbody, mirrors and wheels is used. The flow equations of this test case are similar to those of eq. (10) where instead of the energy equation, the Spalart–Allmaras turbulence model equation should be solved and the turbulent viscosity is added to the bulk one. The development of the adjoint equations are similar to those for the heat transfer problem but, since this is a shape optimization problem, grid sensitivities ($\delta x_k/\delta b_n$) are involved in the computation. Moreover, the turbulence model should be differentiated appropriately and contributes to both the field adjoint equations and the gradient computation. Further details can be found in [14, 15].

Regarding the UQ study, uncertainties are introduced in the flow conditions and the QoI is the drag coefficient (C_D). For the flow without uncertainties, with freestream velocity equal to 38.89 m/s and zero yaw angle, C_D=0.31705. The uncertain variable is the freestream velocity magnitude with μ_v=38.89 m/s and σ_v=1m/s. The UQ results are summarized in Table 5.

Chaos Order	μ_{C_D}	σ_{C_D}
2	0.31695	$9.78433 \cdot 10^{-4}$
3	0.31563	$2.26329 \cdot 10^{-3}$
4	0.31650	$1.43895 \cdot 10^{-3}$

Table 5: DrivAer car case: Mean value and standard deviation of C_D on the baseline geometry for different chaos orders. The freestream velocity is the uncertain variable.

Once the UQ study has been completed, next step is to use the adjoint method to optimize its shape under uncertainites. The objective function to be minimized during the design under uncertainties is that of eq. (4), with κ=1.

The convergence histories of the optimization runs are shown in fig. 5. Recall that, for the optimization without uncertainties, each optimization cycle costs two equivalent flow solutions (EFS; this accounts for the numerical solution of the Navier-Stokes equations or their adjoint which have, more or less, the same cost). On the other side, for the design under uncertainties, each optimization cycle has a cost equal to either 6 EFS (for q=2; 3 flow and 3 adjoint solutions) or 8 EFS (for q=3). It is also important to note that, for the two examined chaos orders, the resulting optimal/robust solutions are very close each other. Regarding the overall reduction of the QoI, in the design without uncertainties a reduction of 5% in C_D is achieved after 9 cycles (or 18 EFS). A reduction of 1.5% is achieved in $\hat{F}$ after 4 cycles (or 32 EFS). From fig. 6, an area of increased pressure is present over the rear window of the car on the optimal shapes, which results to a reduction in the drag force.

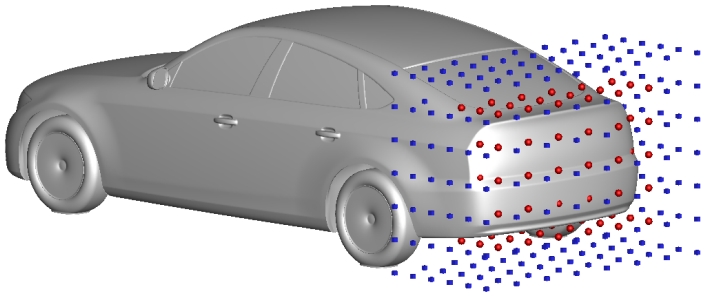

Figure 4: DrivAer car case: The rear part of the car is parameterized using volumetric B–Splines. The control points of the lattice are responsible for the deformation of the enclosed part of the car surface. During the optimization, the red points are allowed to move while the blue ones remain fixed (in two layers) in order to ensure C1-continuity of the shape during the optimization.

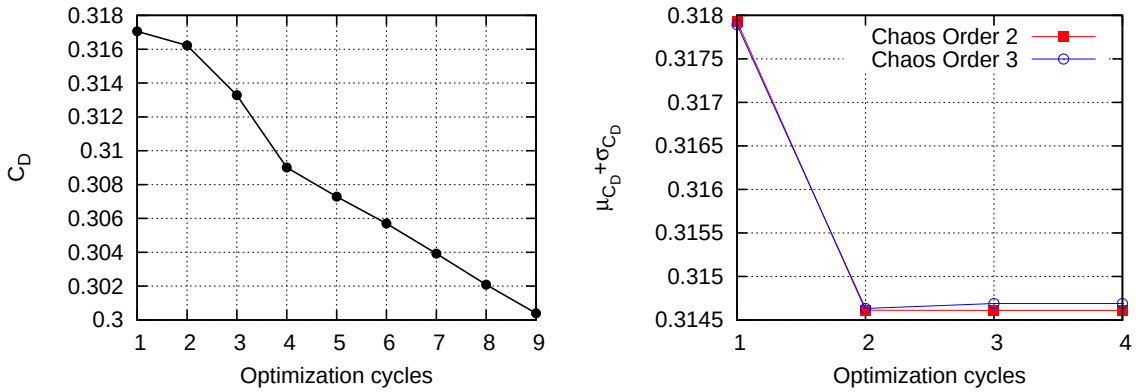

Figure 5: DrivAer car case: Convergence history of the optimization without (left) and with (right) uncertainties for chaos order q=2 and q=3.

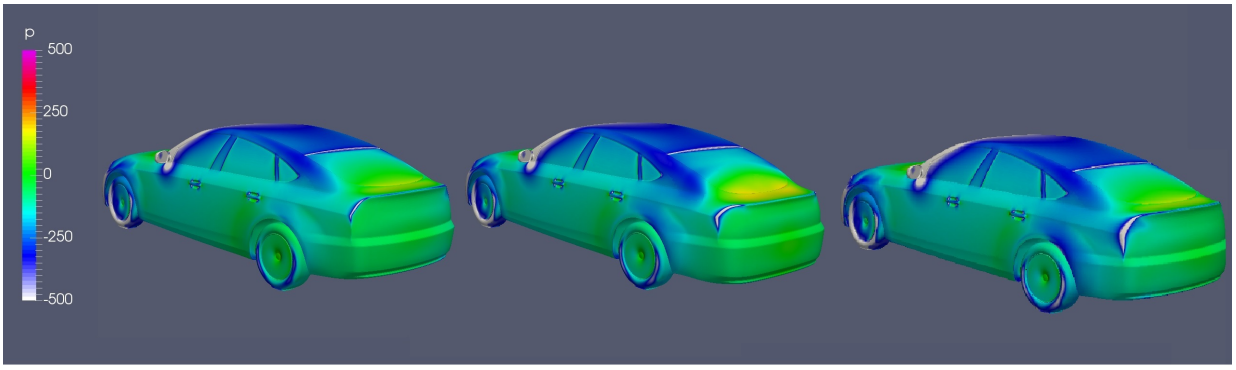

Figure 6: DrivAer car case: Static pressure distribution on the baseline geometry (left), the optimal car without considering uncertainties (middle) and the optimized with uncertainties (q=2).

5 CONCLUDING REMARKS

A reliable method for dealing with optimization under uncertainties was presented. The UQ needed for the computation of the statistical moments of the QoI is based on the non–intrusive PCE. The continuous adjoint technique is used to compute the gradient of the QoI w.r.t. the design variables at the Gaussian nodes, the weighted combination of which is the gradient of the objective function to be used in the gradient–based design under uncertainties. The proposed method was demonstrated into two cases, i.e. the optimization under uncertainties of a lid–driven cavity for maximum heat transfer and of a car model for minimum drag. In either case, significant improvement in the objective function was observed. The integration of the adjoint technique in the robust design algorithm is straightforward when the non–intrusive PCE is used. This technique can be used in any engineering application where uncertainties (either in operating conditions or shape imperfections) are present, since in the non–intrusive PCE technique the analysis software is used as a black–box.

6 ACKNOWLEDGEMENT

The first author is an Early Stage Researcher (ESR) in the IODA project which has received funding from the European Union's Horizon 2020 Research and Innovation Programme under the Marie Sklodowska–Curie Grant Agreement No. 642959. The authors acknowledge Mr. I.–K. Katsaros, Mech. Engineer, NTUA, who contributed in the first phase of the cavity problem. The second application was supported by computational time granted from the Greek Research & Technology Network (GRNET) in the National HPC facility - ARIS - under project ID "PR002012-DuUFluid".

REFERENCES

[1] A.G. Liatsikouras, V.G. Asouti, K.C. Giannakoglou, G. Pierrot, and M. Megahed. Aerodynamic shape optimization under flow uncertainties using non–intrusive polynomial chaos and evolutionary algorithms. In *UNCECOMP 2017*, Rhodes Island, Greece, 2017.

[2] A.G. Liatsikouras, V.G. Asouti, K.C. Giannakoglou, and G. Pierrot. Aerodynamic shape optimization by considering geometrical imperfections using polynomial chaos expansion and evolutionary algorithms. In *EUROGEN 2017*, Madrid, Spain, 2017.

[3] S. Asmussen and P.W. Glynn. *Stochastic simulation: Algorithms and analysis*. Stochastic Modelling and Applied Probability. Springer New York, 2007.

[4] W.J. Morokoff and R.E. Caflisch. Quasi-Monte Carlo integration. *Journal of Computational Physics*, 122(2):218–230, 1995.

[5] M.D. McKay. Latin hypercube sampling as a tool in uncertainty analysis of computer models. In *Proceedings of the 24th Conference on Winter Simulation, Arlington, Virginia, USA*, 1992.

[6] E.M. Papoutsis-Kiachagias, D.I. Papadimitriou, and K.C. Giannakoglou. Robust design in aerodynamics using 3rd-order sensitivity analysis based on discrete adjoint. application to quasi-1D flows. *International Journal for Numerical Methods in Fluids*, 69(3):691–709, 2012.

[7] D.I. Papadimitriou and K.C. Giannakoglou. Third-order sensitivity analysis for robust aerodynamic design using continuous adjoint. *International Journal for Numerical Methods in Fluids*, 71(5):652–670, 2013.

[8] C. Lacor and S. Smirnov. Non-deterministic compressible Navier–Stokes simulations using polynomial chaos. In *ECCOMAS 2008*, Venice, Italy, 2008.

[9] M.B. Giles and N.A. Pierce. An introduction to the adjoint approach to design. *Flow, Turbulence and Combustion*, 65(3-4):393–415, 2000.

[10] I.S Kavvadias, E.M. Papoutsis-Kiachagias, and K.C. Giannakoglou. On the proper treatment of grid sensitivities in continuous adjoint methods for shape optimization. *Journal of Computational Physics*, 301:1–18, 2015.

[11] D. Xiu and G.E. Karniadakis. The Wiener–Askey polynomial chaos for stochastic differential equations. *SIAM Journal on Scientific Computing*, 24(2):619–644, 2002.

[12] G.H Golub and J.H. Welsch. Calculation of Gauss quadrature rules. *Mathematics of Computation*, 23(106):221–230, 1969.

[13] A.I. Heft, T. Indinger, and N.A. Adams. Experimental and numerical investigation of the Drivaer model. In *ASME 2012 Fluids Engineering Division Summer Meeting collocated with the ASME 2012 Heat Transfer Summer Conference and the ASME 2012 10th International Conference on Nanochannels, Microchannels, and Minichannels*, Puerto Rico, USA, 2012.

[14] E.M. Papoutsis-Kiachagias and K.C. Giannakoglou. Continuous adjoint methods for turbulent flows, applied to shape and topology optimization: Industrial applications. *Archives of Computational Methods in Engineering*, 23(2):255–299, 2016.

[15] E.M. Papoutsis-Kiachagias, S. Porziani, C. Groth, M.E. Biancolini, E. Costa, and K.C Giannakoglou. Aerodynamic optimization of car shapes using the continuous adjoint method and an RBF morpher. In *EUROGEN 2015*, Glasgow, UK, 2015.